Microfluid Nanofluid (2007) 3:591–602
DOI 10.1007/s10404-007-0148-5

RESEARCH PAPER

Transient response analysis and modeling of near wall flow conditions in a micro channel: evidence of slip flow

Helmut Neff · Antonio Marcus Nogueira Lima · Fernanda Cecília Correia Lima Loureiro · Luiz Alberto Luz de Almeida

Received: 2 October 2006 / Accepted: 14 December 2006 / Published online: 3 February 2007

Abstract An experimental tool for determination of the near wall transport parameters in a micro channel, supported by flow simulation, is presented. The method is based on the transient flow response due to convective diffusion, in absence of specific adsorption. An approximately step-function type temporal solute concentration variation serves as the input signal. The associated response signal of a surface plasmon resonance sensor, acting as an integral part of a micro channel, has been taken as the output signal. It provides the flow-dependent change of the NaOH solute concentration in the channel within the optical detection and near wall distance interval $0 < d < 0.5$ μm. The temporal signal evolution and response time, until an initially plain aqueous solution is replaced by the solute, varies inversely with solute concentration and flow rate. In the asymptotic limits, the near wall forced convective and diffusive channel transit times, along with the associated velocities, can be extracted and separated. A low convective near wall flow speed would account for 100% adsorption efficiency. The validity of the scaling relation for Fickian diffusive transport has been confirmed by experiments. Convective near wall flow reveals a distorted parabolic flow profile. This indicates relaxation of the no-slip condition, and presence of slip flow. Neither boundary layer formation, nor near wall micro turbulences have been observed. Eventually, a compact mathematical transient flow model, outlined in the Laplace domain for the electrical equivalent analogue circuit and applicable to the convective diffusion equation, has been developed for the flow transients.

Keywords Micro fluidics · Convective diffusion · Transport parameters · Diffusion length · Slip flow · Modeling

H. Neff (✉) · A. M. N. Lima · F. C. C. L. Loureiro
Department of Electrical Engineering (DEE),
Federal University at Campina Grande (UFCG),
Avenida Aprigio Veloso, 882 58.109-970 Campina Grande,
PB, Brazil
e-mail: hneff@get2net.dk

A. M. N. Lima
e-mail: amnlima@dee.ufcg.edu.br

L. A. L. de Almeida
Department of Electrical Engineering (DEE),
Federal University of Bahia (UFBA),
Salvador, BA, Brazil

1 Introduction

Recent developments of sensitive and compact instrumentation for life science and environmental analytical applications, also known as lab-on-chip or micro total analysis systems (μ-TAS), have attracted considerable technological and economic attention (Guber et al. 2004; Hiukko et al. 2003; Manz et al. 1990). The technology crucially relies on and comprises controlled fluid transport of liquid analytes to and from a sensing transducer, using integrated micro fluidic devices. Commonly, electronically readable analytical signals are generated in a channel type microfluidic cell, where the analyte is passing between two closely spaced planar plates. The transducer function can be established by surface functionalization of one of the channel walls, employing physicochemical-binding and/or biochemical/biological recognition principles, including formation of antibody-antigen complexes. A further

important application of micro channels is chromatographic separation, where pressure-driven flow through conduits can lead to large solute dispersion (Dutta et al. 2006).

Particle transport within fluids, containing dissolved solutes, is appropriately treated by a combination of convective diffusion (CDE) with hydrodynamic Navier–Stokes (NSE) equations. This covers the interplay of two different, superimposed and perpendicular transport mechanisms: molecular diffusion of the solute out of the bulk fluid towards the channel walls, mainly driven by local concentration gradients, and forced convective, hydrodynamic transport of the solute within the solution along the channel. The total mass flow is given by the sum of both fluxes. The CDE and NSE represent non-linear second order partial equations, with variable coefficients. The solutions shall provide both, the temporal development and spatial distribution of solute concentration $c(x, y, z, t)$, along with its velocity profile. Solving of the CDE and the NSE is mathematically demanding, largely related to difficult boundary and initial conditions. Both, boundary and initial conditions depend critically on the nature of physico- and biochemical processes of the solute(s) in solution and their interaction at or on bioactive interfaces, acting as sensing or functionalized elements.

The mathematical difficulties to establish closed analytical solutions, suggest the use of either purely numerical finite element (FE), or implementation of simplifying approximations. An example is the earlier approach to quantify solute transport within a micro fluidic flow channel, adopting analytical concepts and approximations, initially developed for the electrochemical thin layer cell (Matsuda 1967; Sjoelander and Urbaniczky 1991). Convective diffusive transport of ions in rectangular channels has been mathematically treated in detail previously (Moldoveanu and Anderson 1984), although restricted to stationary conditions. A series solution of the transient CDE for the rotating disc electrode in the time domain, employing the Laplace representation, has been outlined recently (Santhanagopalan and White 2004). Likewise, a computational fluid dynamics approach to treat mass transport and macromolecular adsorption kinetics under non-stationary conditions has been published (Jenkins et al. 2004).

Under certain conditions, micro- and macrofluidic conduits reveal substantially different, yet not fully understood hydrodynamic properties (Mahulikar and Herwig 2006). The reduced geometric dimensions of micro channels account for more complex flow pattern, particularly near wall boundaries, where the high surface-to-volume ratio supports increased influence of surface effects. They may originate from micro surface roughness and friction, micro air bubble and/or boundary layer formation, local electric fields by adsorbed charges and impurities, and interfacial potential gradients. A further important and related, but rarely considered issue addresses the wetting properties at the wall surface, whether behaving hydrophilic or hydrophobic and, eventually, the influence and magnitude of capillary forces. Under these conditions, the no-slip flow condition commonly holds in a modified form, but is insufficiently treated by conventional theory. At very small dimensions, reliable flow profile measurements are difficult to perform, and demand rather complex experimental investigations and set-ups.

Finite element calculations of micro flow systems are now established, but frequently lack experimental verification. Presently, only a limited number of experimental micro flow investigations have been reported. High-resolution velocity profiles in micro channels, recorded by image velocimetry (PIV), revealed significant deviations from ideal flow behavior, particularly at flow boundaries and interfaces, and in close vicinity to channel walls. At distances < 5 μm, boundary layer effects, flow oscillations, as well as vortex like fluid motions have been resolved (Park et al. 2003; Shinohara et al. 2004; Sinton and Li 2003), while at larger wall distances the parabolic profile was largely maintained. The PIV technique, however, is not suited to reliably probe the near-surface region at distances at or below the μm range. Here, an attempt has been made, to evaluate near wall fluid transport parameters with high spatial resolution by experiment. Quantitative data are important, since they determine the sensing characteristics and adsorption efficiency of the flow cell, but also affect and distort measurements of kinetic binding constants.

The transient response of surface plasmon resonance (SPR) recordings in absence of surface adsorption has been used to extract quantitative solute transport data, with the optical instrument serving as an integral part of the micro flow channel. The optical sensing range of the SPR phenomenon comprises a precisely defined wall distance interval, at which flow parameters are extracted. It is placed at approximately 0.5 μm, or about half of the operating wavelength of the SPR spectrometer. The associated physical function and operation conditions of the surface plasmon resonance spectrometer (Neff et al. 2006), and instrument, employed in this work have been reported in detail elsewhere (Melendez et al. 1996). A reevaluation of mass transport and surface reactions in microfluidic systems, relevant to surface plasmon

resonance experiments, has been published recently (Gervais and Jensen 2006). Both, convective and diffusive flow velocities superimpose, and differ substantially. This difference can be explained and elaborated on bases of the above mentionned convective diffusion equation that applies to the flow system under investigation. This is the aim of this work, as demonstrated in the experimental section. By varying solute concentration and flow velocity/flow rate both, diffusive and convective transport parameters can be explored directly. Eventually, the experimental findings are compared and supported by simulated data, employing a novel CDE solution approach that relies on its Laplace representation within the frequency domain.

2 Theoretical aspects and data extraction

The general dynamic vector form of the differential convective diffusion equation follows ultimately from the continuity equation

$$\frac{\partial c}{\mathrm{d}t} = -\mathrm{div}(j) \tag{1}$$

where j is the mass flow and describes the motion of an ionic or macromolecular solute particle in a solvent stream (Levich 1962):

$$\frac{\partial c}{\mathrm{d}t} = D\Delta c - (v \cdot \mathrm{grad}) \cdot c \tag{2}$$

c represents the temporal and spatial concentration distribution of the solute in the solvent. D is the diffusion coefficient of the solute, and v the temporal and spatial velocity profile of the solution. Source and sink terms are not included, since specific solute adsorption is absent. Also, electrokinetic contributions are not considered.

Under stationary conditions, $\frac{\partial c}{\mathrm{d}t} = 0$, the CDE reduces to:

$$D\Delta c = (v \cdot \mathrm{grad}) \cdot c \tag{3}$$

which can be solved analytically for simple geometries. Subtraction of the stationary form from the dynamic CDE yields the temporal variation $\frac{\partial c}{\mathrm{d}t}$. Tracking of the temporal evolution $\Delta\tau_{\mathrm{resp}}$, until stationary conditions and chemical equilibrium are established, provides an experimental exploration method of the CDE. Defined initial conditions are required to numerically extract the transient response. Consequently, the application of a solute concentration variation step Δc as an input quantity is providing $\frac{\Delta c}{\Delta\tau_{\mathrm{resp}}}$, which varies with c, v, D, and temperature as well as the channel geometry.

In the asymptotic limit, for $v \to 0$, at finite c, the CDE transforms into the molecular diffusion equation:

$$\frac{\partial c}{\mathrm{d}t} = D\Delta c \tag{4}$$

The NSE can be related to the CDE in absence of a dissolved solute, i.e., at $D = 0$, and replacement of the solute (analyte) concentration c by the solvent density ρ. In the absence of the diffusive term, for $c \to 0$ at finite v, (2) transforms into the first Navier–Stokes equation, to compute the velocity profile:

$$\frac{\partial \rho}{\mathrm{d}t} = -\mathrm{grad}(\rho v) \tag{5}$$

For incompressible fluids, the NSE reads as

$$\rho\frac{\partial v}{\mathrm{d}t} = \mu\Delta v - \rho v \cdot \mathrm{grad}(v) - \mathrm{grad}(P). \tag{6}$$

P is the fluid pressure in the cell, and μ the viscosity of the solution. Thus, evaluation of the dynamic flow response $\frac{\Delta c}{\Delta\tau_{\mathrm{resp}}}$ in the asymptotic limits, for $v \to 0$ and $c \to 0$, shall provide information on the diffusive and convective flow properties in the channel.

Furthermore, the Poiseuille equation represents a simple analytical solution to the NSE for tubular and rectangular channel with low aspect ratios. The ideal velocity profile across the channel cross section is parabolic, with $v_{\mathrm{t}}(z) = 0$ at the wall surface $(z = \frac{h}{2})$, comprising the no-slip condition:

$$v_{\mathrm{t}}(z) = \left(z^2 - \frac{h^2}{4}\right)\frac{1}{2\mu}\frac{\partial p}{\mathrm{d}x} \tag{7}$$

v_{t} is the tangential velocity component in the flow direction z, $\frac{\partial p}{\mathrm{d}x}$ is the pressure gradient along the cell length, h the cell height. The total mass flux j of the solute out of the solution onto the active sensing area is given by two contributions

$$j = cv - D \cdot (\mathrm{grad}c). \tag{8}$$

Calculation of j requires solving of the CDE for both $c(x, y, z, t)$ and the solution velocity $v(x, y, z, t)$. The mass flux is not a constant quantity, but varies with position, within the channel.

According to Moldoveanu and Anderson (1984) and Sjoelander and Urbaniczky (1991), the overall analyte flux can be estimated by introducing the concept of

reduced transit time $\tau_R = \frac{\tau_{CD}}{\tau_{Diff}}$, defined as the ratio of applied uniform and diffusive transit times of the solute through the cell, while moving along and perpendicular to the sensing surface, respectively. As mentioned earlier, the approach has been introduced earlier, as an attempt to substantially simplify the mathematical determination of *j* from the CDE, towards a description of mass transfer in the electrochemical thin layer cell. Under steady state conditions, the normalized, relative particle flux or overall adsorption efficiency as a global quantity of a flow cell, is given approximately as (Sjoelander and Urbaniczky 1991)

$$J_{re} = 1.47\tau_R^{2/3}. \quad (9)$$

To determine J_{re} both above mentioned quantities must be provided.

Here, the transient response method, usually applied to experimentally evaluate the dynamic properties of electrical/electronic circuits, has been adapted to address a micro fluidics problem. An electrical circuit with unknown dynamic properties can be considered as a black box, comprising two in- and output terminals. Stimulation of the circuit by a step function, Heaviside type electrical excitation $H(t)$ (unit step signal) at its input terminals, which defines the initial conditions, will cause a transient response signal at the output terminal. Hence, the temporal evolution of the output signal is determined by the dynamics of the set of differential equations that apply to the electrical equivalent circuit in the box. For example, a simple first order electric circuit/system would provide an exponentially varying decay/rise time as the transient response. Likewise, as indicated in Fig. 1a, when the flow channel is considered as a black flow box, stimulated by a well-defined step flow input signal, the transient cell response of an appropriately selected output signal will be modified by the dynamics of the equation system, governing fluid transport within the channel. The technical approach to simulate micro fluidic systems, using equivalent electrical analogue circuit modeling, comparable to the SPICE platform, has been evaluated before (Chatterjee and Aluru 2005). Transient response analysis also has been used to study diffusion through membranes (Nguyen et al. 1993). The transient SPR signal, taken in this work in close vicinity to the wall surface within the distance interval < 0.5 μm, exploits local flow properties via its solute concentra-

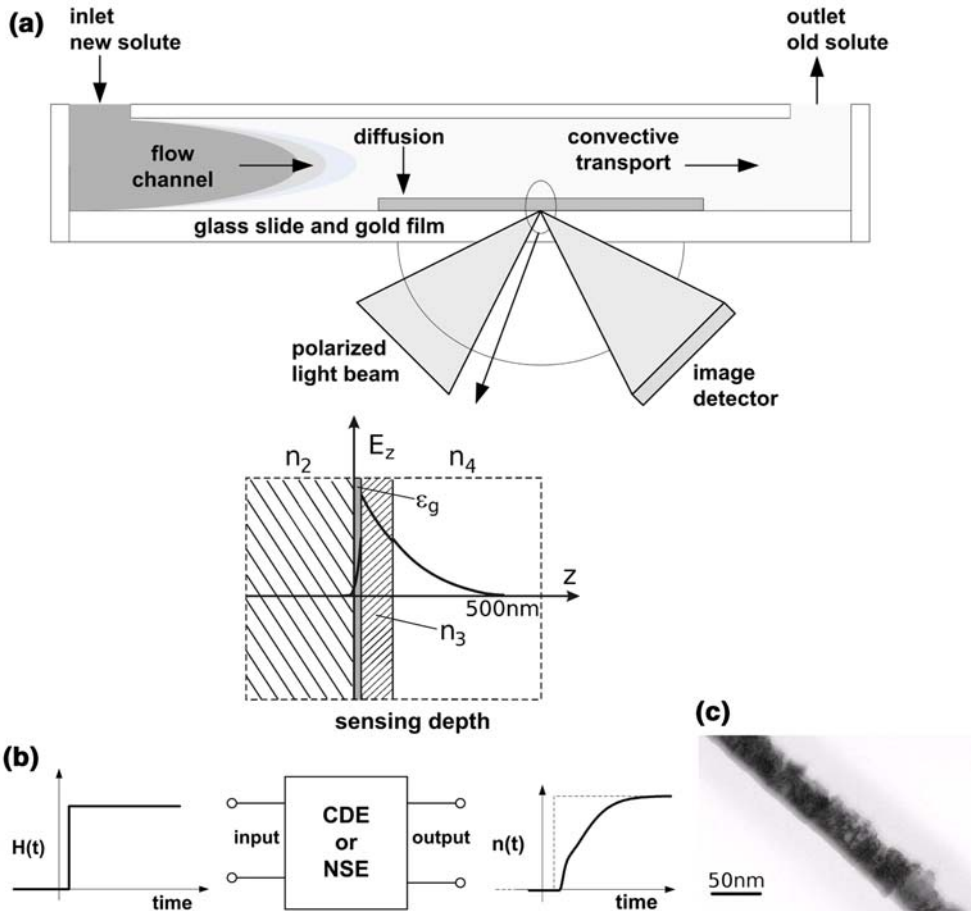

Fig. 1 **a** Schematic arrangement of the flow cell with its integrated SPR-sensor. Flow and solute transport conditions are indicated in the figure. The magnified bottom section illustrates the near wall optical sensing range, defined by the penetration of the SPR-evanescent wave field into the solution, up to 0.5 μm. Approximately 70% of the signal originate within a distance interval of 0.2 μm from the gold surface. **b** Black box schematics of the input–output relation. The step function type flow input signal applies at the left flow cell entrance, the (optical) output signal is taken at the SPR sensor. **c** Cross-sectional high resolution transmission electron microscope (TEM) image of the channel wall forming gold surface, depicting rms roughness modulations around 3–5 nm

tion dependent temporal refractive index variations $\Delta c(\Delta n[t])$.

3 Experimental aspects

A sketch of the experimental set-up, comprising a SPR sensor with angular interrogation, is illustrated in Fig. 1 a. The optical sensor with its attached semi-transparent gold-film and sensing surface is placed at the lower base plate of the channel. The counter plate is made from Teflon, and comprises the flow in-and outlet. The local optical SPR probing range into the flow channel is indicated in the lower, cut-out magnified figure. It corresponds to the decay length and extension of the evanescent optical wave field into the solution, where flow properties are sampled. Flow conditions of the aqueous solution, containing Na^+ and OH^- ions, are considered steady state, and laminar at given low Reynolds numbers within the channel, but turbulent near inlet and outlet. The (input) solute concentration profile across the channel can be represented by Gaussian type distribution function. It varies with time and location along the channel extension. Figure 1b illustrates the black-box input–output scheme. The flow input signal approximately corresponds to step-function solute concentration variation with time, $\Delta c(t) = H(t)$. Due to installed short Teflon tubing from the analyte reservoir towards the flow cell, and fluid mixing at the turbulent inlet section, solute dispersion effects that would broaden the input concentration profile can be neglected. Figure 1c illustrates the surface topography of the wall. It is covered with a thin, semitransparent and 50 nm thick polycrystalline gold-film, deposited onto an amorphous polymer substrate. Close inspection of the high resolution transmission electron microscopy (TEM) image of Fig. 1c, reveals that the wall surface exhibits only weak nano-scaled surface roughness modulations, due to outgrowth of gold micro crystals, at rms-magnitudes of 3–5 nm. The channel surface is free of microscopic flow obstacles, which could trigger micro turbulences in the near surface region.

The experiments were performed as follows: first, pure-water was pumped through the flow channel, and the output signal recorded with the SPR-instrument. The pump was shut-off, and the flow interrupted. The water filled tubing end was inserted into the well, containing the NaOH solute ions at various molar concentrations, and the pump restarted. This created a sharp interface between both solution although no separating air-gap was applied. Subsequently, the pump was turned on, driving the new solution through the Teflon tubes into the flow channel, where it slowly replaced the originally contained water-solution by diffusive and convective solute transport. SPR-output data, defining the transient response time, were recorded as function of flow rate and solute concentration, until steady state condition is reached.

Both, diffusive and convective transport of solute ions out of the bulk solution flow towards, and along the sensing surface superimpose, and cause a temporal change of the ion concentration within the SPR sensing volume $\Delta c(t)$. Over a time period $\Delta\tau$, a stable uniform ion concentration distribution and chemical equilibrium is established within the channel. The transient output signal, provided by the SPR spectrometer, delivers the temporal variation of the concentration-dependent refractive index within the sensing volume $\Delta c(\Delta n[t])$, either governed by diffusive or convective transport, τ_{Diff} and τ_{cv}, or a combination thereof. For moderately high solute concentrations, the associated refractive index variation scales strictly linear, thus providing a direct measure for the concentration within the near wall region.

The SPR cell response time, taken as the output signal, was determined as function of solute concentration variations Δc and volume flow rate f, using the 10–90% SPR signal variation criterion, as well as their asymptotic values at $f \rightarrow 0$ and $c \rightarrow 0$, respectively. As mentioned earlier, in the former case, the diffusive transit time and associated diffusion length are explored, at which solute particles are traveling perpendicular to the sensing surface, until the sensing volume (in front of the sensing surface) is filled. In the latter case, the forced convective response can be extracted, where the solute particles travel preferably lateral, in close vicinity of the sensing surface, until the sensing volume is filled, while the diffusive flow contribution can be neglected.

The temporal resolution is approximately 2 s, which is the minimum sampling rate at sufficiently low noise level. Broadening of the response signal also can be caused by interdiffusion across the liquid–liquid interface during transport through the teflon tubings, which can take up to 30 s. However, at low solute concentration, as employed for convective transport measurements, this effect should be neglectable.

Experiments have been performed at ambient temperature (25°C), using the SPREETA surface plasmon resonance evaluation kit, and attached flow cell, described in detail elsewhere (Melendez et al. 1996). Due to its robust and stable design, the device is easy to operate. Supplying suited peripheral instrumentation and optimized operation conditions both, noise level and sensor drift can be maintained at very low levels,

utilizing a temporal resolution of 2 s. The flow cell length is set at 11 mm, the width set at 1.2 mm and the cell height comprises 0.75 ± 0.05 mm, comprising a cell volume of 10 μL at a dead volume of 1 μL p.a. grade NaOH solutions, prepared from nano-pore filtered, de-ionized water have been used for the experiments, leaving a hydrophilic surface. Molar concentrations of the analyte solution are varying within the range 0.001M $< c <$1M. pH-stabilizing buffer solutions have not been employed during the experiments, since this would have changed the solute concentration and composition. The absence of pH stabilization required fast recordings with fresh prepared solutions.

The NaOH solute has been chosen, since the refractive index variation with concentration, $\frac{\Delta n}{\Delta c}$, from OH^--ions is substantially higher than in presence of Cl^--ions of alkaline NaCl solutions. This allows for precise, low-noise response time recordings at very low (mM) concentrations. A precision peristaltic pump (Ismatek ISM 832A) has been used during the experiments. Small pressure fluctuation during pump operation did not affect recording accuracy. It should be mentioned that the experiments required very careful handling and cleaning of all, the sensing gold surface and the Teflon tubing for analyte transport to the cell, in order to minimize slow signal drift effects, while maintaining the SPR-signal noise at sufficiently low and stable values $\leq 5 \times 10^{-6}$RIU (refractive index units).

3.1 Transient flow modeling

Numerical FE-simulations of the partial differential flow equations in two- or three-dimensions are numerically demanding and time consuming for applications with high spatial resolution. Compact, easy to implement flow models, thus, are useful to fast elaboration of the flow dynamics of microfluidic devices, but also allow fast integration with other micro-mechanical and microelectronic models, employed in commercial simulators. An appropriate mathematical model has been derived earlier (Santhanagopalan and White 2004) to obtain the concentration transient response of a rotating disk electrode, and adapted in this work. Following a similar approach to that adopted in Santhanagopalan and White (2004), for distances sufficiently close to the film surface, we propose that the nonlinear equations for transport mechanisms be approximated by a set of two independent linear differential equations of the form

$$\sum_{i=1}^{M} a_i \frac{\mathrm{d}^i}{\mathrm{d}t^i} c_d(t) = u(t) \tag{10}$$

$$\sum_{i=1}^{N} b_i \frac{\mathrm{d}^i}{\mathrm{d}t^i} c_c(t) = u(t) \tag{11}$$

and thus

$$c(t) = k c_c(t) + (1-k) c_d(t) \tag{12}$$

where $c_d(t)$ and $c_c(t)$ are the time-domain diffusion and convection concentrations, respectively, is the normalized solute concentration and k is a constant to define the contribution of each transport mechanism. The parameters a_i and b_i are coefficients, M and N are the orders of the differential equations. Taking the Laplace transform of the above set of equations, assuming repeated roots for the denominator polynomials, and rearranging and parameters we obtain

$$\frac{C_c(s)}{U(s)} = H_c(s) = \frac{1}{\sum_{i=1}^{N} b_i s^i} \tag{13}$$

$$\frac{C_d(s)}{U(s)} = H_d(s) = \frac{1}{\sum_{i=1}^{M} a_i s^i} \tag{14}$$

Briefly, a simple black-box model is proposed, and related to the aforementioned mathematical approach for the two different diffusion and convection transport mechanisms. For mathematical simplicity, these two phenomena are considered as independent. This allows introduction of a linear operator being both, linear and homogeneous, which obeys the principle of superposition.

This last assumption facilitates the parameter estimation procedure, since each phenomenon features a different transient time scale. The proposed operator, or transfer function, defines an input–output dynamic relation between the pressure-driven new solute concentration $u(t)$ and the SPR measured concentration $\Delta c(\Delta n[t])$ in a microfluidic channel. This transfer function $H(s)$ is equal to the Laplace transform $C(s)$ of the output signal $c(t)$ divided by the Laplace transform $U(s)$ of the input signal $u(t)$. $H(s)$ can be written as weighted sum of two different transfer functions

$$H(s) = \frac{C(s)}{U(s)} = k H_c(s) + (1-k) H_d \tag{15}$$

k is a constant, representing the proportion between the convective transport transfer function $H_c(s)$ and the molecular diffusion transfer function $H_d(s)$. To obtain $H_c(s)$ and $H_d(s)$, we assume a wave-like propagation of the concentration front in a microfluidic channel, introduced earlier (Gervais and Jensen 2006). The present model adapts a single-phase

electrical transmission line as an appropriate electrical analogue model for channeled fluid transport, obtained by cascading several identical first order sections

$$H_c(s) = \frac{\omega_c^N}{(s+\omega_c)^N}, \quad H_d(s) = \frac{\omega_d^M}{(s+\omega_d)^M} \tag{16}$$

where ω_c and ω_d are angular cut-off frequencies given in radians/s, N and M are integer numbers, equal or greater than one, which are related to the length of the channel and the dominating transport mechanism, respectively. Equation 16 can be used to build a lumped parameter representation of an electrical transmission line. It describes the propagation of an electric field along a metallic conductor as a function of frequency. It can be found in advanced textbooks for electrical engineers. Here we use the same equation as an electrical analogue to describe the propagation of a diffusive front and concentration profile through a channel at velocity v. The numbers N and M are free adjustable parameters to adjust and match to the experimental data. The larger the channel, the longer is the transport delay, and the higher are N and M. As a parameter estimation procedure, we first applied a very low concentration step $u(t)$ of NaOH solute and assumed $N = M = 3$ and $k = 1$, neglecting the diffusion contribution to the transient response and obtaining $\omega_c = 0.142$ rad/s. Subsequently, a higher concentration step $p(t)$ of NaOH solute was applied, assuming $k = 0.5$. This indicates the same contribution for both, diffusion and convection, obtaining $\omega_d = 0.02$ rad/s.

The proposed model can be easily integrated into P-SPICE-type and MATLAB/SIMULINK simulators.

4 Results and discussion

Figure 2a and b depict representative variations of SPR signals (in RIU values), as a function of time for 0.1 and 0.006 m NaOH solutions, respectively. Note that the SPR-output signal variation Δn (in RIU) is proportional to the input concentration variation, Δc. While the former data set at large c reveals a single, sharp temporal SPR response variation, and rapid signal increase over a time scale of 30–40 s, at very low concentration two different, superimposed response features at similar magnitude, but substantially different time scales are resolved: an initial, fast response of around 20 s, followed by a much slower temporal variation, extending up to 300 s. The former feature is attributed to a dominating diffusive, the latter to the convective contribution. Individual 10–90% response rise times are indicated in the figure.

Figure 3 outlines the recorded 10–90% response times $\Delta\tau_{resp}$, as a function of NaOH solute concentration c, depicted in a log–log representation. Data have been taken at constant volume flow rate of 444 μL/min. For comparison, the originally recorded linear plots are included in the insets for both, NaOH and NaCl solutions.

Presented response times have been obtained by averaging over nine data sets. Due to a much higher noise level, data scattering with σ-values of 46 s is large at very low concentrations. Recording accuracy, with σ = 4.1 s, improves substantially at high solute concentrations. It should be noted that the alkaline solution reveals a slightly shorter response time of 30 s at high, but could not be recorded and extended with sufficient resolution towards the low concentration limit. There are clearly three different flow regions resolved for the NaOH solution: a region of constant SPR response $\Delta\tau_{resp} = 34 \pm 4.1$ s at high NaOH concentrations, with $c > 0.1$; a transition region, with the molar concentration varying at $0.1 < c < 0.01$, featuring a steady increase of the response time and, eventually, a stable region, at very low concentrations. The molar detection limit for NaOH solutions has been determined to $c = 0.002$. At $c < 0.01$, the response time remains stable at $\tau_{resp} = 234 \pm 41$ s, independent of the solute concentration. Considering the channel length of

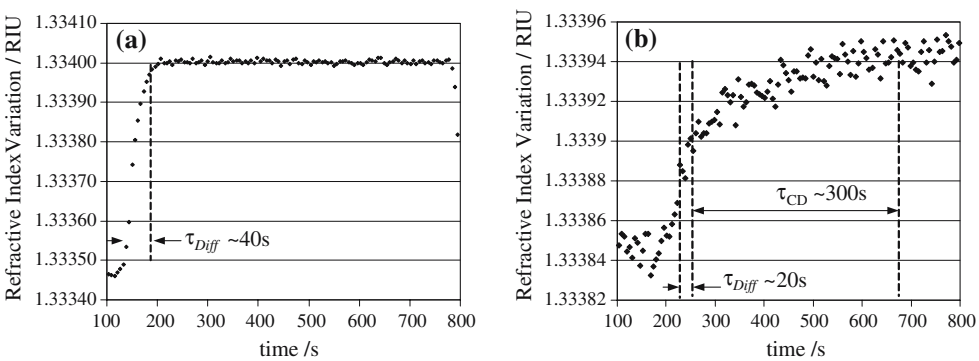

Fig. 2 **a** Transient response of the near wall refractive index variation $\Delta n(t)$ for a 0.1 m NaOH solution, indicating a single rise-time. **b** Transient response of the near wall refractive index variation $\Delta n(t)$ for a 0.006 m NaOH solution, indicating two different rise-times

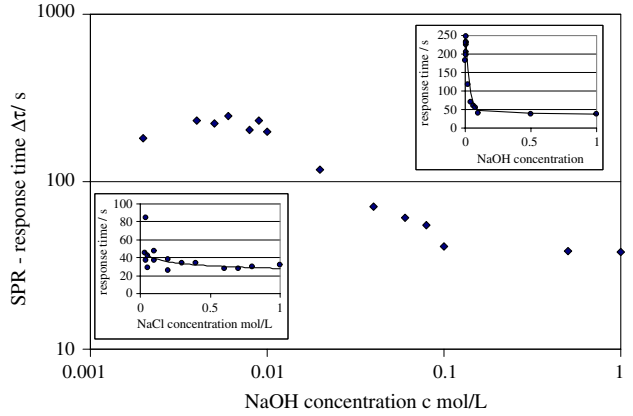

Fig. 3 Transient response rise time $\Delta\tau$ of the near wall refractive index variation, taken from the 10 to 90% signal variation criterion, as function of solute concentration, displayed in log–log representation. *Right* and *left insets* depict the original linear data sets, recorded for NaOH and NaCl solutions

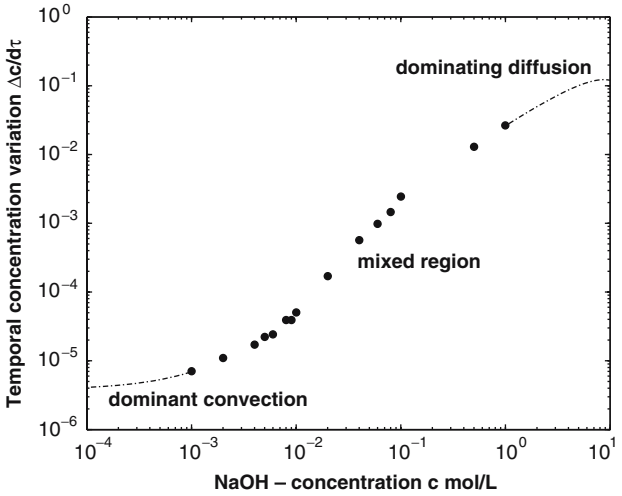

Fig. 4 Experimentally determined variation and shape of the dynamic part of the CDE, $\Delta c/\Delta\tau$, as function of the solute concentration. The asymptotic characteristics are indicated by *broken lines* where saturation appears either for diffusive or convective behavior

11 mm, the associated (averaged) near wall hydrodynamic flow speed within the wall distance from 0 to 0.5 μm at the given flow rate is determined to $v_{HD} = 0.047$ mm/s.

Figure 4 illustrates the experimentally determined shape and solution of the left side of the CDE, according to Eq. 2. The broken lines indicate the expected approximate asymptotic behavior of the *s*-shaped function. The kinetic part $\Delta c/\Delta\tau$ is shown in log–log representation as a function of NaOH solute concentration c, as taken from the data set of Fig. 3. Three different flow regions were resolved, exhibiting different slopes: at high concentration, where large values for $\Delta c/\Delta\tau_{resp}$ persist, the diffusive contribution dominates, with $D\Delta c > (v\cdot \text{grad})\cdot c$. In the very low concentration regime, an increased response time accounts for a very small value $\Delta c/\Delta\tau_{resp} \rightarrow 0$, where diffusive and convective flows are balanced, thus $(v\cdot \text{grad})\cdot c \approx D\Delta c$. This conclusion is supported by the almost identical magnitudes of diffusive and hydrodynamic flow contributions, illustrated in the temporal signal evolution of Fig. 2b. In the intermediate region, a steady transition between both flow quantities appears. As indicated in the data set of Fig. 2b, the extrapolated hydrodynamic transit time τ_{HD} at $c \rightarrow 0$, determines to 234 s. Taking into account the experimentally obtained diffusive transit time; this would result in a near surface reduced transit time $\tau_R = \tau_{HD}/\tau_{Diff} = 1.39$. In view of an earlier flow analysis of Moldoveanu and Anderson 1984, this would correspond to a local, relative near wall flux efficiency of 100%.

The near wall flow speed squares with the applied flow rate, and associated uniform flow velocity v_u, respectively. This is illustrated in Fig. 5, where the experimentally determined v_{HD} is plotted against the applied v_u in the channel. v_u is obtained from the applied volume flow rate, taking into account channel length and volume. Figure 6 shows the estimated slip velocity v_{slip} and slip length δ_{slip} obtained at an uniform flow velocity of 9 mm/s (540 μl/min) determined to 0.07 mm/s and 0.73 μm. For this estimate, it was considered that the experimental flow profile is also parabolic, and obeys the same slope near the surface. For the uniform flow velocity, it has been found,that <5 mm/s is threshold value, below which slippage dis-

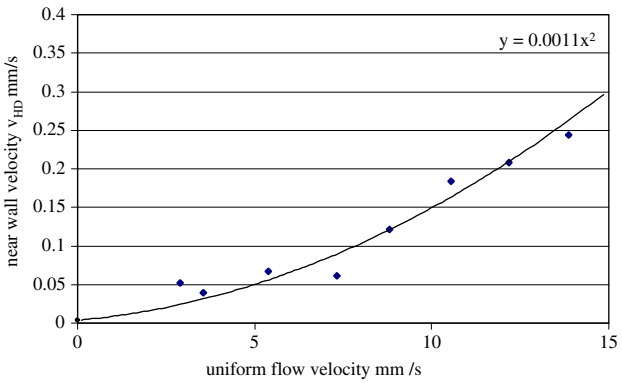

Fig. 5 Experimental obtained near wall flow speed as function of applied uniform velocity v_u, taken from the volume flow rate. The *solid line* to the data points illustrates the best polynomial fit, with parabolic variation. The line along the *x*-axis corresponds to and depicts the magnitude of the associated diffusion velocity

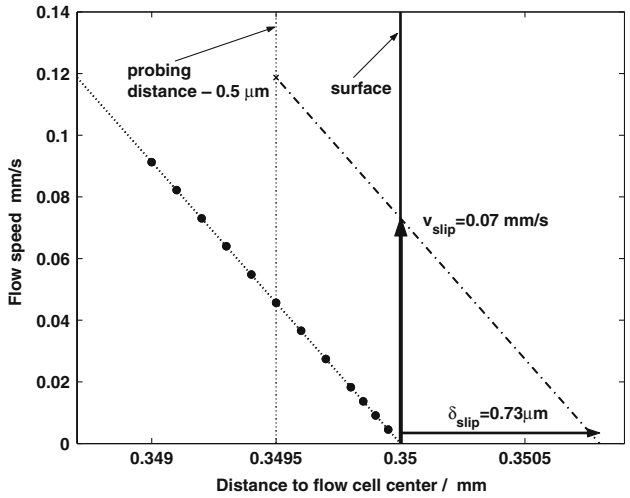

Fig. 6 Estimated slip velocity and slip length at an uniform flow velocity of 9 mm/s (540 μl/min)

appears. For higher uniform flow speeds the slip length increases non-linearly.

The related, convective response time $\Delta\tau_{HD}$ scales inversely with v_u, following a power law, as indicated in the Fig. 7. For comparison, the inset reveals the estimated hydrodynamic transit time, calculated on the basis of the Poiseuille equation for a wall distance of 0.5 μm. Distinct differences exist between both data sets: the estimated transit/response times for the purely parabolic flow profile are about a factor 2 higher than the experimentally determined τ_{HD}-values. In other words, the ideal parabolic flow profile yields about a factor 2 lower near wall flow speed, compared to the experimentally determined quantity. Second, the exponent in the power law is exactly –1 for the parabolic profile, but is determined slightly higher than –1.2172 for the recorded data. The solid line represents an automatically generated best-fit to the experimental data, employing a power law to define the exponents. The standard deviation (R^2) is 0.8771 for the experimental values and exactly 1 for the ideal parabolic profile.

The temporal concentration variation $\Delta c/\Delta\tau$ in the high concentration limit for a 0.1 m NaOH solution, as function of volume flow rate is depicted in Fig. 8. The inset reveals the original data set, where the response time reveals a clearly non-linear increase with decreasing flow rate, along with an associated exponent of –0.69. The large difference to the exponent of –1.21 in Fig. 7, recorded at very low solute concentrations, illustrates the different dominating transport mechanisms. It is important to note that $\Delta c/\Delta\tau$ scales linearly with f, thus establishing easy extrapolation towards $f = 0$ (or $u = 0$), to extract the value of the (aforementioned concentration independent) diffusive transit time. In accordance with the solution to Eq. 4, for the given flow cell geometry, the diffusive transit time until the (concentration) equilibrium is established and is determined from $\Delta c/\Delta\tau_0 = 0.0029$, to $\tau_{Diff} = 172.4\ s$. Considering the channel height and diffusion length of 0.75 mm, the associated diffusion velocity across the

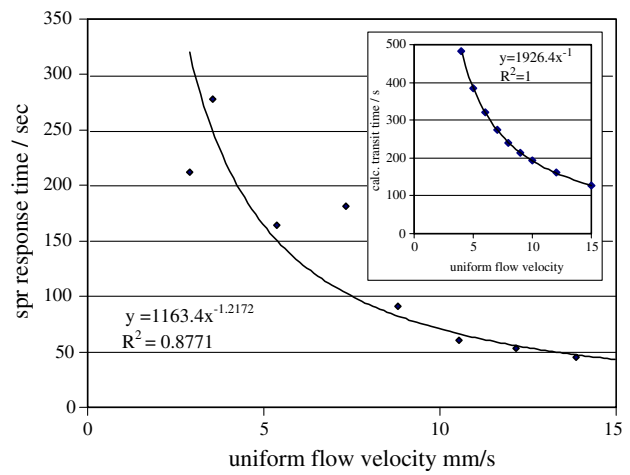

Fig. 7 Variation of SPR response time as function of applied uniform flow velocity, associated to the data set of Fig. 5. The *solid line* corresponds to the best fit, employing a power law at an exponent of –1.21. *Inset* reveals the variation, obtained for the ideal parabolic flow profile from the Pouseille equation for a wall distance of 0.5 μm, revealing an exponent of –1

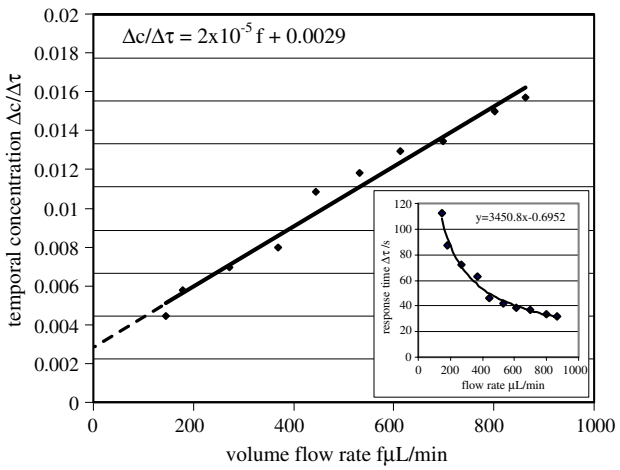

Fig. 8 Experimentally determined variation and shape of the dynamic part of the CDE, $\Delta c/\Delta\tau$, as function of volume flow rate for determination of the diffusive transport parameter for 0.1 molar NaOH solution. The *broken line* indicates extrapolation to $f = 0$, which provides the diffusive transit time. *Inset* reveals the associated original data set of the SPR response time as function of flow rate

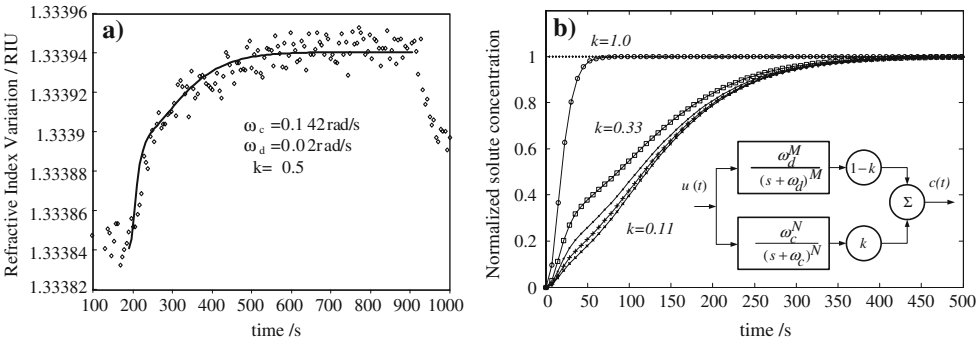

Fig. 9 **a** Comparison of the simulated transient, shown in a *solid line*, with the recorded low concentration data taken from Fig. 2b. **b** Set of simulated transients for different adjustable parameters *k*. The *inset* illustrates the equivalent electrical analogue circuit in the Laplace domain, pertaining to the CDE

channel is obtained to $v_{\mathrm{Diff}} = 0.0043\ mm/s$, independent of the applied flow rate.

Eventually, Fig. 9a illustrates an example of a simulated response, utilizing the Laplace representation of the CDE, depicted as a fit to the experimentally obtained transient at low solute concentration, as shown in Fig. 2b. With appropriately selected fitting parameters, all recorded transients are accurately reproduced. Figure 9b illustrates a set of flow transients, calculated for different fitting parameters *k* in the Laplace representation, and attributed to low and high solute concentrations. The inset illustrates the associated electrical analogue circuit, employed in the simulation.

The present experimental findings concern several different critical transport issues, related to solute diffusion and forced convective flow. A theoretical approach, addressing the diffusive transit time, has been used earlier (Sjoelander and Urbaniczky 1991), and based on the Fickian diffusion scaling relation. However, no experimental verification, regarding the accuracy of the selected estimation method has been provided by the authors. The expression originates from statistical mechanics considerations, and is given as $\tau_{\mathrm{Diff}} = h^2/D$, where *h* is the cell height, or mean square particle displacement, and *D* the diffusivity of the solute. This concept has been widely used, and applied to theoretically determine the diffusion mechanism of water through nanotubes (Striolo 2006). Thus, within this approximation, the output quantity crucially depends on the selected *D*-value. There are substantial variations among the different ions, which sensitively depend on the size and properties of their surrounding hydration shell. For macromolecules, *D* is approximately inversely scaling with the molar weight.

As mentioned before, comparison with the SPR response of NaCl solutions indicated that a high fraction of the output signal originates from the presence of OH^- ions in the solution. Also, OH^- ion diffusivity and mobility values are approximately a factor-3 higher, compared to their Na^+- counter ions, thus implying faster transport into the near surface sensing volume. It is therefore reasonable, to select the associated transport coefficient (Tuckerman et al. 2006) with $D^{OH-} = 3.12 \times 10^{-5}\ cm^2/s$, and not the about 30% lower combined ion pair diffusivity. With this approximation, and using the cell height $h = 0.75$ mm, the diffusive transit time calculates to $\tau_{\mathrm{Diff}} = 180.3$ s. Within an error margin of 5%, this value agrees with the experimentally determined $\tau_{\mathrm{Diff}} = 172.4$ s. The present findings thus provides both, a direct experimental verification/confirmation of the above mentioned diffusion scaling relation, along with a validation of the presented approach to experimentally determine diffusive transport parameters.

Furthermore, the experimental results of the present work directly confirm the presence of convective flow conditions in the near wall regime $\leq$ 0.5 μm, along with the absence of a boundary layer. Experimental evidence for the possibility of such a stable boundary layer in a micro channel, where the tangential velocity component drops to zero within wall distances up to 5 μm, was given in the PIV data of Fig. 8 of Shinohara et al. (2004). On the other hand, shortly outside of this no-slip region, below and at μm ranges, the tangential flow velocity reveals comparable magnitudes under conditions, pertaining to and displayed in Fig. 5 of this work. However, it should be noted that PIV recordings reveal a limited spatial resolution, most likely less than 1 μm. The agreement with the results of independent experimental micro flow observations, obtained with a different technical set-up, thus confirms the present findings and associated data extraction method. It also supports the quality of the selected experimental route.

However, the majority of experimental observations regarding convective flow properties in micro channels, available to us, indicated distinct distortions, compared to the ideal parabolic flow pattern. For example, close inspection of the pressure-driven flow pattern in very narrow channels in the PIV data of Fig. 3 (Sinton and

Li 2003) reveals a distinct maximum and subsequent flow reversal in the near wall region at very low tangential flow velocities. This behavior cannot be explained, and disagrees with the Poiseuille equation. Also, recorded flow profiles, as shown in Fig. 18 of the work of Park et al. (2003) indicated substantially higher flow velocities outside of the channel center, towards the walls, than would be expected of a purely parabolic flow profile. This can be understood as a relaxation of the no-slip condition, and would support our experimental findings on the possibility of higher tangential flow velocity at wall distance $\approx$ 0.5 μm, exceeding at least a factor of 2 the calculated parabolic near wall flow speed. The effect appears even more pronounced, if one refers and limits the sensing distance from the wall to $\approx$ 0.2 μm, where up to 70% of the recorded SPR signal originates. Under these conditions, the ideal parabolic profile, and connected no-slip condition, would lead at the same flow rate to a transit time of approximately 1,050 s, which is substantially higher than the recorded value of 234 s.

At present, there is no full understanding, regarding the origin of scaling effects and deviations from the ideal parabolic hydrodynamic flow profile near channel walls. Variations of viscosity along the flow direction have been considered recently (Mahulikar and Herwig 2005). Also, surface effects have been invoked to play a crucial role, and the relaxation of the no-slip condition has been attributed to the presence of hydrophilic or hydrophobic surfaces (Choi et al. 2003), and surface roughness or intermolecular interactions for very smooth surfaces (Zhu and Granick 2002). Direct evidence for the existence of rate dependent slip flow has been reported recently (Zhu and Granick 2001). The recorded slip length, which is proportional to the slip velocity (Choi et al. 2003) was shown to scale non-linearly with the applied flow rate/flow velocity, similar to the results presented in Fig. 5 of this work. Therefore, we attribute the observed high near wall velocity, primarily to the presence of slip flow at the wall surface, which distorts the ideal low velocity parabolic profile within the SPR-sensing volume. According to previous investigations on slip at smooth surfaces (Zhu and Granick 2001), there exist at least two scenarios for microscopic interpretaion of the non-linear characteristics: (1) the fluid viscosity might vary with the wall distance or (2) the presence of gas/vapor bubbles that nucleate in the presence of shear at solid surface (de Gennes 2002). Whether one of these explanations applies to the present experimental results is not clear at present.

A final and important issue relates to the accuracy to which the overall cell adsorption efficiency of macromolecular solutes onto a binding sensing surface can be determined, using Eq. 9. As illustrated in the earlier-mentioned approach (Sjoelander and Urbaniczky 1991), calculation of the diffusive transit time on the basis of the Fickian scaling relation firmly relies on the data accuracy of the input parameters, namely the diffusion coefficient and cell height. Both quantities reveal severe limitations. For example, the exact height h of a micro fluidic flow cell is affected by the selected sealing arrangement. Frequently, soft elastomeric O-ring sealings are used, which tend to deform in a poorly known amount under an applied sealing pressure load. The effect is particularly critical for very narrow flow channel arrangements. Mechanical deformations within the 10% range are easily imposed, which severely limits the accuracy to which h can be determined. Also, required diffusivity values in aqueous solution are often uncertain. While those for the simple ions are well documented, the huge and increasing amount of proteins and other biomaterials used in biochemical research, exhibiting large molar weight variations, prevent determination of individually accurate numbers. The present approach, to experimentally assess ionic diffusive transit times, can be adapted to determine macromolecular diffusivities. The method does not rely on uncertain input parameters, but on relatively easy-to-perform diffusive transit time measurements τ_{Diff}, using the relation $D = h^2/\tau_{\mathrm{Diff}}$. The achievable accuracy largely depends on the given instrumental signal-noise ratio. Measurements should be feasible with any state-of-the art SPR spectrometer, attached to an appropriately designed flow channel or cell, where the cell height is precisely known.

5 Conclusions

The transient flow of an aqueous solution has been exploited, towards analysing flow conditions in a microchannel. Flow properties are ascribed to the convective diffusion equation, transforming into the Navier–Stokes equation at low-solute concentration and the diffusion equation at low flow speed. The evanescent wave of a surface plasmon resonance set-up has been used as the sensing probe, penetrating approximately 0.5 μm into the channel. From the temporal signal evolution, the near wall forced convective and diffusive channel transit times have been extracted. Analysis of the data reveals validity of the Fickian scaling law. The method allows precise determination of solute diffusion coefficients in aqueous solution. Above a critical flow rate, near wall convec-

tive flow speed substantially exceeds Pouseuille flow for an ideal parabolic profile, and is indirectly attributed to the presence of slip flow.

Acknowledgments The authors thank FAPESQ/PB and CNPq for the award of research and study fellowship during the course of these investigations.

References

Chatterjee AN, Aluru NR (2005) Combined circuit and device modeling and simulation of integrated microfluidic systems. J Microelectromech Syst 14:81–95

Choi CH, Westin JA, Breuer KS (2003) Apparent slip flows in hydrophilic and hydrophobic microchannels. Phys Fluids 15:2879–2902

Dutta D, Ramachandran A, Leighton Jr. DT (2006) Effect of channel geometry on solute dispersion in pressure driven micro fluidic systems. Microfluid Nanofluid 2:275–290

Gervais T, Jensen KF (2006) Mass transport and surface reactions in microfluidic systems. Chem Eng Sci 61:1102–1121

Guber AE, Heckele M, Hermann D, Muslija A, Saile V, Eichhorn L, Gietzelt T, Hoffmann W, Hauser P, Tananiwa J, Gerlach A, Gottschlich N, Knebel G (2004) Microfluidic lab-on-chip systems based on polymers-fabrication and application. Chem Eng J 101:447–453

Hiukko K, Kostianinen R, Kotiaho T (2003) Introduction to micro-analytical systems: bioanalytical and pharmaceutical applications. Eur J Pharm Sci 20:149–171

Jenkins J, Prabhakarpandian B, Lenghaus K, Hickman J, Sundaram S (2004) Fluidics resolved estimation of protein adsorption kinetics in a biomicrofluidic system. Anal Biochem 331:207–215

Levich VG (1962) Physico-chemical hydrodynamics. Prentice Hall, Englewood Cliffs

Mahulikar SP, Herwig H (2006) Physical effects in laminar microconvection due to variations in incompressible fluid properties. Phys Fluids 18:073601

Mahulikar SP, Herwig H (2005) Theoretical investigation of scaling effects from macro-to-microscale convection due to variations in incompressible fluid properties. Appl Phys Lett 86:0141051

Manz A, Graber N, Widmer HN (1990) Miniaturized total chemical analysis systes: a novel concept for chemical sensing Sens. Actuators B Chem 1:244–248

Matsuda H (1967) Zur Theorie der stationaeren Strom-Spannungskurven von Redox Elektrodenreaktionen in hydrodynamischer Voltametrie: laminare Rohr- und Kanalstroemungen. Electroanal Chem 15:325–336

Melendez J, Carr R, Bartholomew DU, Kukanskis K, Elkind J, Yee S, Furlong C, Woodbury R (1996) A commercial solution for surface plasmon sensing. Sens Actuators B 35:212–216

Moldoveanu S, Anderson JL (1984) Amperometric response of a rectangular channel electrode. J Electroanal Chem 175:67–77

Neff H, Zong W, Lima AMN, Borre M, Holzhueter G (2006) Optical properties and instrumental performance of thin gold films near the surface plasmon resonance. Thin Solid Films 496:688–697

Nguyen QT, Gref R, Clement R, Lenda H (1993) Differential permeation-Part 1: a method for the study of solvent diffusion through membranes. Colloid Polym Sci 271:1134–1142

Park H, Pak JJ, Son SY, Lim G, Song I (2003) Fabrication of a micro channel integrated with inner sensors and the analysis of its laminar flow characteristics. Sens Actuators A 103:317–329

Santhanagopalan S, White RE (2004) Series solution to the transient convective diffusion equation for a rotating disk electrode. J Electrochem Soc 151:150–153

Shinohara K, Sugii Y, Aota A, Hibara A, Tokeshi M, Kitamori T, Okamoto K (2004) High speed micro PIV measurements of transient flow in microfluidic devices. Meas Sci Technol 15:1965–1970

Sinton D, Li D (2003) Electroosmotic velocity profiles in microchannels. Colloids Surf A Physicochem Eng Asp 222:273–283

Sjoelander S, Urbaniczky C (1991) Integrated fluid handling system for biomolecular interaction analysis. Anal Chem 63:2338–2345

Striolo A (2006) The mechanism of water diffusion in narrow carbon nanotubes. Nano Lett 6:633–639

Tuckerman ME, Chandra A, Marx D (2006) Structure and Dynamics of OH^-. Acc Chem Res 39:151–158

Zhu Y, Granick S (2002) Limits of the hydrodynamic no-slip boundary condition. Phys Rev Lett 88:106102

Zhu Y, Granick S (2001) Rate dependent slip of Newtonian Liquid at smooth surfaces. Phys Rev Lett 87:096105

de Gennes PG (2002) On fluid/wall slippage. Langmuir 18:3413–3414